Partial breaking of the Coulombic ordering of ionic liquids confined in carbon nanopores

Ryusuke Futamura, Taku Iiyama, Yuma Takasaki, Yury Gogotsi, Mark J. Biggs, Mathieu Salanne, Julie Ségalini, Patrice Simon and Katsumi Kaneko

Supplementary information

Content

1. Intra-molecular structure of EMI and TFSI ions

In Figure 2a, the experimental ERDF of EMI-TFSI bulk liquid display 3 peaks for distances below 0.40 nm, located at 0.14, 0.27 and 0.38 nm. The peak located at 0.14 nm corresponds to the intramolecular distances of C-N, C-C and N-S inside IL molecules. The peaks located at 0.27 and 0.38 nm respectively correspond to the nonbonding S···F interaction and the nonbonding S···C interaction intra TFSI ion. Small deviations between the experimental and simulated profiles for these distances are caused by the presence of several conformers for each ion in the bulk liquid as reported previously[1] while we use rigid molecular models in the HRMC procedure. The slight disagreement between the experimental RSF and the simulated one of Fig. 1c in the *s*-range of 15 to 25 nm^{-1} is therefore attributed to these deviations.

2. Anion-cation and cation-cation structures of EMI-TFSI in bulk liquid and in the nanopores

HRMC derived electron radial distribution functions for anion-cation (**a**) and cation-cation (**b**) pairs in bulk liquid (top), 1-nm pore (middle) and 0.7-nm pore (bottom) are shown in Fig S2. For the cation-anion ERDF, the intensity of the first peak at 0.55 nm slightly decreases in the case of the 0.7 nm pores compared to that of bulk liquid (Fig. S2a). For the cation-cation ERDF, a deviation of the negative peak intensity at 0.45 nm towards a more positive value is observed in the case of the 0.7-nm pores compared to that of bulk (Fig. S2b). The occupation percent of nearest coordination shell by cations around a cation in 0.7-nm pore is 19 %, being slightly larger than those of bulk liquid (16%) (see Fig. S2 c and e). The breaking effect of the Coulombic ordering for ionic structure around a cation is not as evident as the one observed for TFSI anions in this ionic liquid. This can be attributed to the formation of nonpolar domains of aggregated alkyl chains, which is typical of imidazolium-based ILs[2]. Even if this effect is relatively small for EMI cations due to the short length of the two chains, it introduces a small proportion of pairing between them even in the bulk. The occupation of 12 % in 1-nm pore is smaller than that of bulk liquid, which is caused by adlayer formation on each pore wall with the Coulombic ordering (Fig. S2 d).

3. Detailed explanation for the molecular orientation against *z*-axis with *z*-coordinate of 0.7-nm and 1-nm pores

For the orientational analysis, we assign 3 orthogonal vectors for cations (left) and anions (right) as shown in Fig. 5b. The molecular structure of EMI and TFSI ions can be approximated by a planar shape. Thus we define two in-plane vectors (***L*** and ***S***) and one out-of-plane vector (***T***). For EMI cations, ***L*** is the vector passing through the two N atoms in the imidazolium ring and ***S*** is the normal to ***L*** in the imidazolium ring plane. For TFSI anions, ***L*** is the vector passing through the two S atoms and ***S*** is the vector normal to ***L*** in the S-N-S plane.

Figure 5a shows distribution of EMI ions across the slit pore in 0.7-nm pore. 83 % of EMI cations locate in the central grey region (i). Order parameter changes of ***L***, ***S*** and ***T*** vectors against *z*-axis (Fig. 5c) show that EMI cations have a molecular alignment in which the out-of-plane vector ***T*** of EMI is almost parallel to the pore walls whereas the long and small molecular axes (vectors ***L*** and ***S***) are slanted to pore walls in the gray region (i). The double peaks in the cation distribution (Fig. 5a) at region (i) arise from their preferable orientation in which the ethyl chains are adsorbed on the nearest pore walls as shown in the inset. EMI ions akin to the pore walls in the orange region (ii) contribute only 9 % of the total population. They have a parallel orientation for the vectors ***L*** and ***S*** with respect to the pore walls. The residual EMI cations located between grey and orange regions have their vector ***L*** oriented parallel to pore walls.

Figure 5e shows distribution of TFSI ions across the slit pore in 0.7-nm pore. 78 % of TFSI anions locate in the central grey region (i). Order parameter changes of ***L***, ***S*** and ***T*** vectors against *z*-axis (Fig. 5f) show that the out-of-plane vector ***T*** is oriented parallel to the pore walls whereas the vectors ***L*** and ***S*** have no preferential orientation in this region, as shown in the inset. TFSI ions akin to the pore walls in the orange region (iii) contribute only 4 % of the total population. Their ***L*** and ***S*** are oriented parallel to the pore walls. The residual TFSI anions in the light green region (ii) have a parallel orientation of vectors ***L*** and ***T*** to pore walls.

Importantly, large populations of cations and anions located in the pore center show a perpendicular orientation of their molecular planes with respect to the carbon pore walls, resulting in effective stacking of anion-anion and cation-cation in a pair-wise structure in 0.7-nm pore.

As the ions are distributed along the graphene walls for the larger pore of 1 nm (Fig. 4b), the orientational structure along the *z*-axis is quite different from that in the 0.7-nm pore. EMI cations have three main orientations depending on the *z*-coordinate (Fig.S4a). For the most closely adsorbed cations on the graphene walls (i.e. -0.35 nm < z < -0.27

nm and 0.27 nm < z < 0.35 nm), which represent 20 % of the total population, the molecular planes (i.e. imidazolium ring plane) are almost parallel to the carbon walls. The molecular planes of cations which are located at the center of the 1-nm pore (i.e. -0.13 nm < z < 0.13 nm, which represent 10% of the population of cations) have a nearly perpendicular orientation to carbon pore wall. In the interspace located between the center of the pores and just beside of the most closely adsorbed cations on the graphene walls (i.e. -0.27 nm < z < -0.13 nm and 0.13 nm < z < 0.27 nm), $\boldsymbol{S}$ vectors are slanted to the z-axis although the orientation of $\boldsymbol{L}$ and $\boldsymbol{T}$ vectors gradually change as z-coordinate changes from pore wall sides to the center of the pore.

Similarly, TFSI anions have three main orientations depending on the z-coordinate (Fig. S4b). In the most closely adsorbed anions on the graphene walls (i.e. -0.28 nm < z < -0.23 nm and 0.23 nm < z < 0.28 nm), which are 22% of the total number of anions, the molecular planes which we defined before are nearly parallel to the graphene walls (Fig. S4b). The molecular planes of anions which are located at the center of the 1-nm pore have (i.e. -0.12 nm < z < 0.12 nm, 17% of the total population) display a nearly perpendicular orientation to carbon pore wall. In the interspace between the central region and just beside the most closely adsorbed anions on the graphene walls (i.e. -0.23 nm < z < -0.12 nm and 0.12 nm < z < 0.23 nm), $\boldsymbol{S}$ vectors are slanted to the z-axis although the orientation of $\boldsymbol{L}$ and $\boldsymbol{T}$ vectors gradually change as z-coordinate changes from pore wall sides to the center of the pore.

4. Determination method of the intermolecular structure in pores with HRMC-aided X-ray scattering technique

The system was regarded as three-phases corresponding to the adsorbed molecules (admolecule), the solid carbon, and the vacant pore space. The experimental X-ray scattering intensity (I_{obs}), which also includes the back ground scattering (I_{back}), is the sum of the self-scattering terms of solid (I_{sc}^{s}) and adsorbed molecules (I_{sc}^{a}), small angle X-ray scattering due to the presence of pores (I_{saxs}), and the interference terms between admolecules ($I_{if}^{a\text{-}a}$), solid atoms ($I_{if}^{s\text{-}s}$), and the cross-term between admolecules and solid atoms ($I_{if}^{s\text{-}a}$), multiplied by several correction factors. So, the I_{obs} is given by the following equation (1):

$$I_{\mathrm{obs}} = \frac{k}{n_{\mathrm{sld}}} PGA\{I_{\mathrm{sc}}^{\mathrm{s}} + I_{\mathrm{sc}}^{\mathrm{a}} + I_{\mathrm{if}}^{\mathrm{s-s}} + I_{\mathrm{if}}^{\mathrm{a-a}} + I_{\mathrm{if}}^{\mathrm{s-a}} + I_{\mathrm{SAXS}}\} + A\, I_{\mathrm{back}} \qquad (1)$$

where k and n_{sld} are the coefficients converting the experimental intensity from e. u. (electron unit) to c. p. s., and the number of atoms in a solid phase in the simulation cell, respectively. P, G, and A are the correction factors corresponding to the polarization, the X-ray irradiating volume, and the X-ray absorption, respectively. They depend on the experimental setup[3]. Here we used the ones for transmission method on cylindrical sample with incidentally monochromatized X-ray. I_{back} indicates the scattering from the glass capillary cell. For the in-situ X-ray scattering measurement under electric potentials, the back ground scattering also includes that from the small amount of the bulk electrolyte which is related to the ionic conduction into carbon electrodes. The reduced structure function of the adsorbed system $S_{ad}(s)$, which is the direct structural information extracted from X-ray scattering, is the sum of $I_{if}^{a\text{-}a}$ and $I_{if}^{s\text{-}a}$, divided by the sum of self-scattering terms of a pair of EMI and TFSI ions as shown by the following equation (2):

$$S_{\mathrm{ad}}(s) = \frac{I_{\mathrm{if}}^{\mathrm{a-a}} + I_{\mathrm{if}}^{\mathrm{s-a}}}{\sum_i^n f_i^2} \qquad (2)$$

where f_i is atomic scattering factor of atom i. To obtain $S_{ad}(s)$, at first, the I_{saxs} was subtracted using power law of intensity to s at small angle region (i.e. $I_{saxs} \sim s^{-b}$, here b is a positive constant). Both I_{sc}^{s} and $I_{if}^{s\text{-}s}$ were obtained from the scattering intensity (I_{obs}^{s}) of the carbon sample in vacuum, assuming that no structural change occurs on the carbon framework of CDCs by adsorption of ionic liquids. The I_{sc}^{a} of admolecules is defined as following equation (3):

$$I_{\mathrm{sc}}^{\mathrm{a}} = \sum_m^n f_m^2 + \sum_m^n i_m^{\mathrm{inc}} \qquad (3)$$

where f_m and i^{imc} are the atomic scattering factor and incoherent scattering intensity of mth atom in a pair of EMI and TFSI ions ($m \leq n$). The obtained $S_{ad}(s)$ can then be simulated with molecular configurations of admolecules in the simulation cell by HRMC algorithm.

We assumed a slit pore model for the nanopores of CDC in order to estimate $I_{if}^{s\text{-}a}$. The nanopore structure was determined from an N_2 adsorption isotherm measured at 77 K. The physical width H was approximated with the effective pore size w by the simple relation of $H = w + \sigma_C$, where σ_C was the diameter of a carbon atom.

The interference terms of $I_{if}^{a\text{-}a}$ and $I_{if}^{s\text{-}a}$, which provided an essential information on an adsorbed molecular structure, were calculated by the following equations:

$$I_{if}^{a-a} = \sum_{j_1}^{j_1 \neq j_2} \sum_{j_2} f_{j_1} f_{j_2} \frac{\sin s r_{j_1,j_2}}{s r_{j_1,j_2}} \tag{4}$$

$$I_{if}^{s-a} = 2 \sum_{j} \sum_{k} f_j f_k \frac{\sin s r_{j,k}}{s r_{j,k}} \tag{5}$$

where r is the distance between two atoms. In $I_{if}^{a\text{-}a}$ calculation, the summation is carried out for all pairs of j_1th and j_2th atoms in inter- and intra-admolecules. So $I_{if}^{a\text{-}a}$ is composed of inter- and intra-admolecular interference terms (I_{inter} and I_{intra}, respectively), i.e. $I_{if}^{a\text{-}a} = I_{inter} + I_{intra}$.

In the case of our CDC models, $I_{if}^{s\text{-}a}$ can be replaced by following equation after averaged over carbon atoms in graphene walls:

$$I_{if}^{s-a} = 2\pi \sum_{j} \sum_{l} f_j f_c \rho_s \frac{\cos s r_z}{s^2} \tag{6}$$

where l denotes lth graphene layer, ρ_s is the atomic density of graphene, 38.1 atom/nm^2, r_z is the distance between an atom in an admolecule and the graphene layer and f_c is the atomic scattering factor of carbon.

5. Pore characterization of CDCs

We used two CDCs having different average pore sizes of 0.7 nm and 1 nm, which were evaluated by nitrogen adsorption isotherms at 77 K (Fig. S5a). The average pore sizes were determined by the subtracting pore effect method using α_s plots which is effective for porous carbons. The pore parameters and pore size distribution evaluated with QSDFT calculation[4] are shown in Fig. S5c and b, respectively. The adsorption isotherm of the 0.7-nm CDC is rectangular type, indicating the presence of small micropores. The pore size distribution from QSDFT suggests the presence of micropores whose size is less than 0.7 nm. We determined the average pore size by using the subtracting pore effect method (SPE method[5-11]) with high resolution α_s-plot, leading to 0.7 nm of the average pore size. On the other hand, the 1-nm CDC has both of micropores and mesopores; the micropores peak at 0.85 nm and the mesopores distribute up to 4.3 nm. In this study we mainly discuss EMI-TFSI confined in micropores even in the 1-nm CDC.

The previous studies have evidenced that the average pore sizes from the SPE method can be correlated with the intermolecular structure of adsorbed molecules. Thus, we used this average pore size from SPE method as a good measure of the pore size of CDC samples.

6. Structural analysis of EMI-BF_4 in unpolarized 0.7-nm pores of CDC

In our paper, we mainly discuss the structure of EMI-TFSI inside carbon nanopores because EMI-TFSI is one of the most common ionic liquid. To confirm whether the breaking of Coulombic ordering of ionic liquid inside carbon nanopores is a general phenomenon or not, we analyzed the structure of EMI-BF_4 adsorbed in 0.7-nm pores of CDC with HRMC simulation aided X-ray scattering. In Fig. S3a and b, the experimental ERDFs of EMI-BF_4 ionic liquid in bulk and in 0.7-nm pore, respectively, are shown with open circles. The experimental ERDFs are well matched with simulated ones (black solid lines). The shoulder intensity at 0.44 nm in experimental ERDF of EMI-BF_4 in 0.7-nm pore is evident compared with the signal of bulk liquid. The deconvolution analysis with HRMC simulation reveals that the increase of the shoulder intensity is ascribed to the upward deviation of the first negative peaks of BF_4-BF_4 and EMI-EMI ERDFs around 0.4 nm in 0.7 nm-pore. This evidences the intrusion of co-ions into the counter-ionic coordination shell for EMI-BF_4 ionic liquid, similarly to what was observed for EMI-TFSI ionic liquid in 0.7-nm pores. This effect (intrusion of co-ion into the counter-ionic coordination shell) is less marked for EMI-BF_4 (Fig S3g-j) compared to EMI-TFSI since the ion size of BF_4 is too small to induce an intensive screening effect, and the low electron density contrast between EMI and BF_4 ions results in a lower structural resolution.

The pair-wise structure between co-ions are extracted from simulated snapshots for EMI-BF_4 in bulk ionic liquid and in 0.7-nm pore (Fig S3c, e, d, and f). The ratios of paired anion (or cation) number to total anion (or cation) number are 0.036 for anions (Fig. S3c) and 0.21 for cations (Fig. S3e) in bulk liquid. The ratios increase to 0.21 for anions (Fig. S3d) and to 0.42 for cations (Fig. S3f) in 0.7-nm pores. For this IL, the formation of cation pairs is even more marked compared to EMI-TFSI. This is due to the anion structure, which affects the packing of cations in carbon nanopores. The smaller spherical shape of BF_4, compared to the bulky plate-like TFSI anions, facilitates pseudo cation-cation stacking arrangement. The molecular plane orientation between the paired cations was also analyzed with $< P_2(\cos\theta)>$ in both ILs confined in the 0.7-nm pores. A much larger value is obtained for EMI-BF_4 ($<P_2(\cos\theta)> = 0.54$) than for EMI-TFSI ($<P_2(\cos\theta)> = 0.28$) in the pore. This shows that the imidazolium rings of paired cations tend to adopt a more parallel arrangement in EMI-BF_4.

7. Supplementary Figures (Fig. S1-S8)

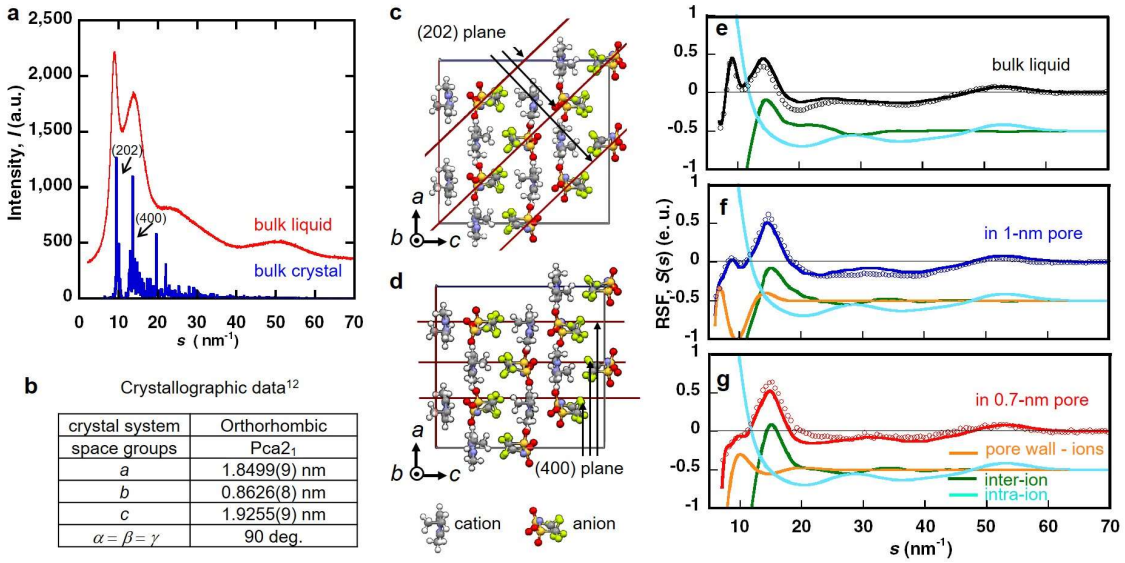

crystal system	Orthorhombic
space groups	$Pca2_1$
a	1.8499(9) nm
b	0.8626(8) nm
c	1.9255(9) nm
$\alpha=\beta=\gamma$	90 deg.

Figure S1| a, XRD profiles of bulk EMI-TFSI in liquid and crystalline states. **b**, Crystallographic data of EMI-TFSI bulk crystals cited from ref.12. (**c**, **d**) Molecular arrangement in (202) **(c)** and (400) **(d)** planes of EMI-TFSI unit cell viewed along *b* axis. The lines indicate (202) (**c**) planes and (400) (**d**) planes. **(e, f, g)** Experimental (open circles) and HRMC-simulated (solid lines) X-ray RSFs of EMI-TFSI in bulk liquid (black) (**e**), EMI-TFSI in 1-nm pores (blue) (**f**) and EMI-TFSI in 0.7-nm pores (red) (**g**). The simulated RSFs related to the inter-ion structure (green), intra-ion structure (sky blue) and intermolecular structure between carbon pore walls and ions (orange) are also shown as solid lines.

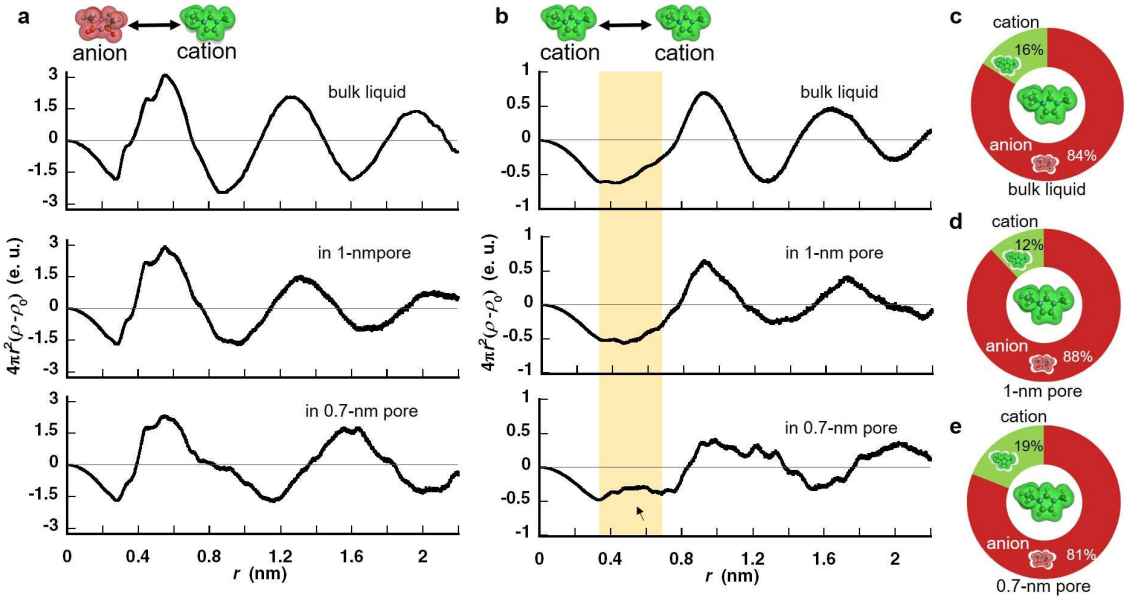

Figure S2| Pore size-dependent anion-cation and cation-cation structures in unpolarized carbon nanopores. (a, **b**) HRMC-derived electron radial distribution functions of anion-cation (**a**) and cation-cation (**b**) in bulk liquid (top), 1-nm pore (middle) and 0.7-nm pore (bottom). (**c**, **d**, **e**) The population in the first coordination shell around an EMI ion in bulk liquid (**c**) and in 1 nm-pore (**d**) and 0.7-nm pore (**e**).

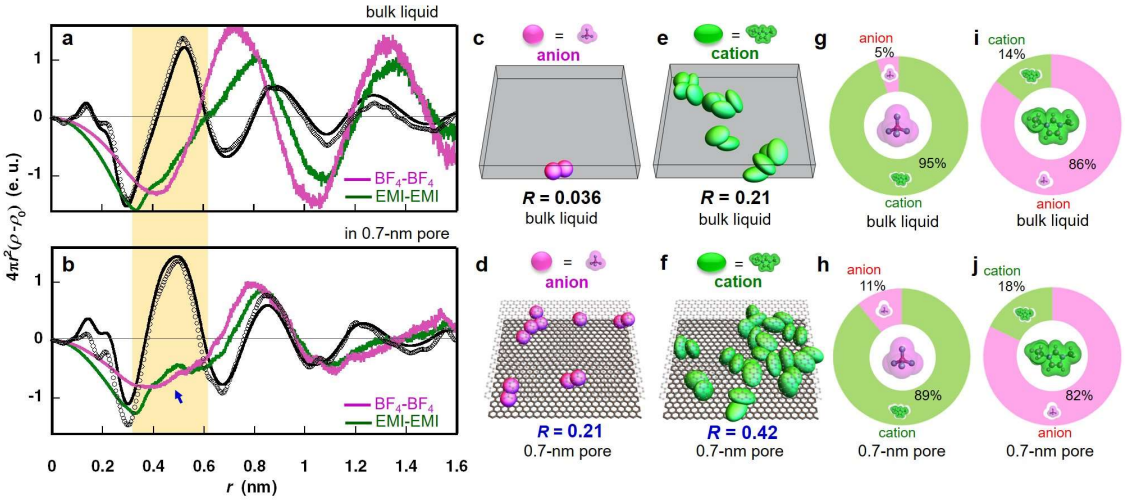

Figure S3|Ionic structure anomalies of confined EMI-BF_4 ionic liquid in unpolarized carbon nanopores of 0.7 nm. (a, b) Experimental and HRMC-simulated electron radial distribution functions (ERDFs) from X-ray scattering of EMI-BF_4 in bulk liquid (**a**) and in 0.7-nm pore (**b**) are plotted with open circles and black solid lines, respectively. Simulated ERDFs of BF_4-BF_4 and EMI-EMI are shown with pink and green lines, respectively. (**c**, **e**) Snapshots of co-ion pairs of anions (**c**) and cations (**e**) for EMI-BF_4 bulk liquid. The co-ion pairs are extracted from the bulk EMI-BF_4 snapshots in 0.7 nm slit spaces. (**d**, **f**) Snapshots of co-ion pairs of anions (**d**) and cations (**f**) for EMI-BF_4 confined in 0.7-nm carbon slit pore. *R* is the ratio of paired anion (or cation) number to total anion (or cation) number. EMI and BF_4 ions are shown as green and pink ellipsoids, respectively. (**g**,**h**,**i**,**j**) The population in the first coordination shell around an EMI (**g**,**h**) ion and a BF_4 (**i**,**j**) ion in bulk liquid (**g**,**i**) and in 0.7-nm pore (**h**,**j**).

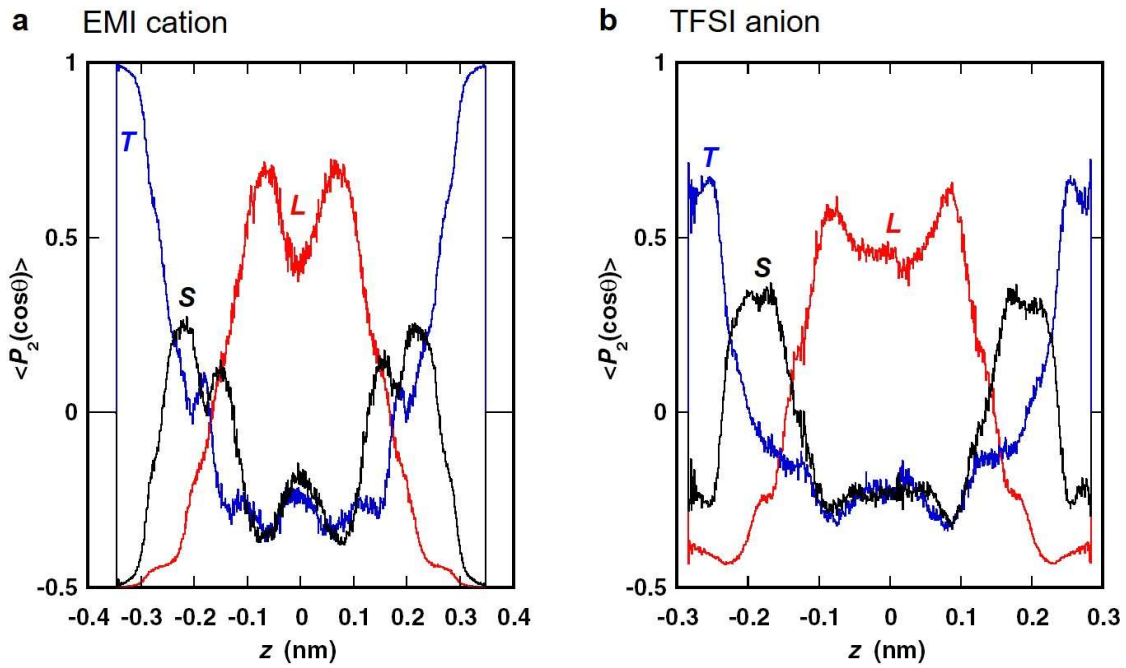

Figure S4| Dependence of molecular orientation of EMI and TFSI confined in 1-nm pore on the coordinate *z* perpendicular to pore walls. (**a**,**b**) Order parameter changes of ***L*** (red), ***S*** (black), and ***T*** (blue) vectors of EMI (**a**) and TFSI (**b**) along the *z*-coordinate in 1-nm slit pore. The definition of ***L***, ***S*** and ***T*** of the cation and anion is given in Fig. 5b. Briefly speaking, the orientational tendency of cations and anions are similar to each other: The orientation depends on three regions (1) near the pore wall, (2) near the central area between two pore walls and (3) the region between (1) and (2). In the region (1) ***T*** tends to be parallel to *z*-axis and both of ***L*** and ***S*** are almost perpendicular to *z*-axis. In the region (2) ***L*** is nearly parallel to *z*-axis and both of ***S*** and ***T*** tend to be perpendicular to *z*-axis. The region (3) has the intermediate tendency between regions (1) and (2)；***S*** is nearly parallel to *z*-axis.

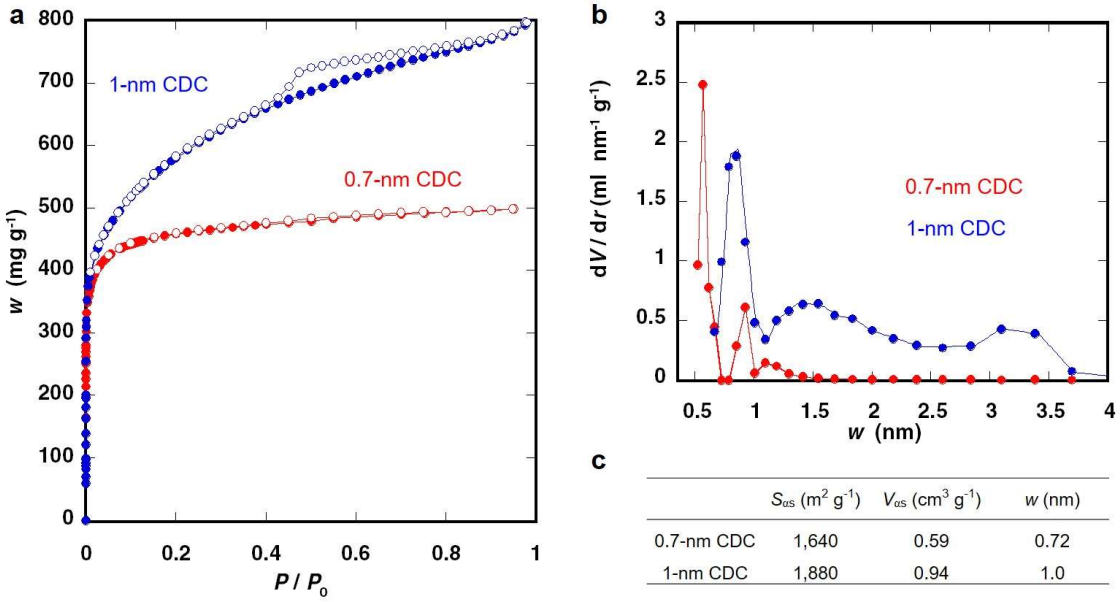

	S_{as} (m^2 g^{-1})	V_{as} (cm^3 g^{-1})	w (nm)
0.7-nm CDC	1,640	0.59	0.72
1-nm CDC	1,880	0.94	1.0

Figure S5| Characterization of porous carbons a, Nitrogen adsorption isotherms of CDC samples with 0.7-nm (red) and 1-nm (blue) average pore size acquired at 77 K. **b**, Pore size distributions of CDC samples evaluated by QSDFT method. **c**, Pore structure parameters of the CDCs determined by subtracting pore effect (SPE) method. Here, S_{as}, V_{as}, and w are the surface area, pore volume, and pore width, respectively, which are determined by SPE method using high resolution α_s-plot of nitrogen adsorption isotherm. The SPE method gives the surface area without overestimation derived by the BET method. The average pore size from the SPE method is obtained from $2V_{as} / S_{as}$, which often provides a reasonable scale of carbon micropores.

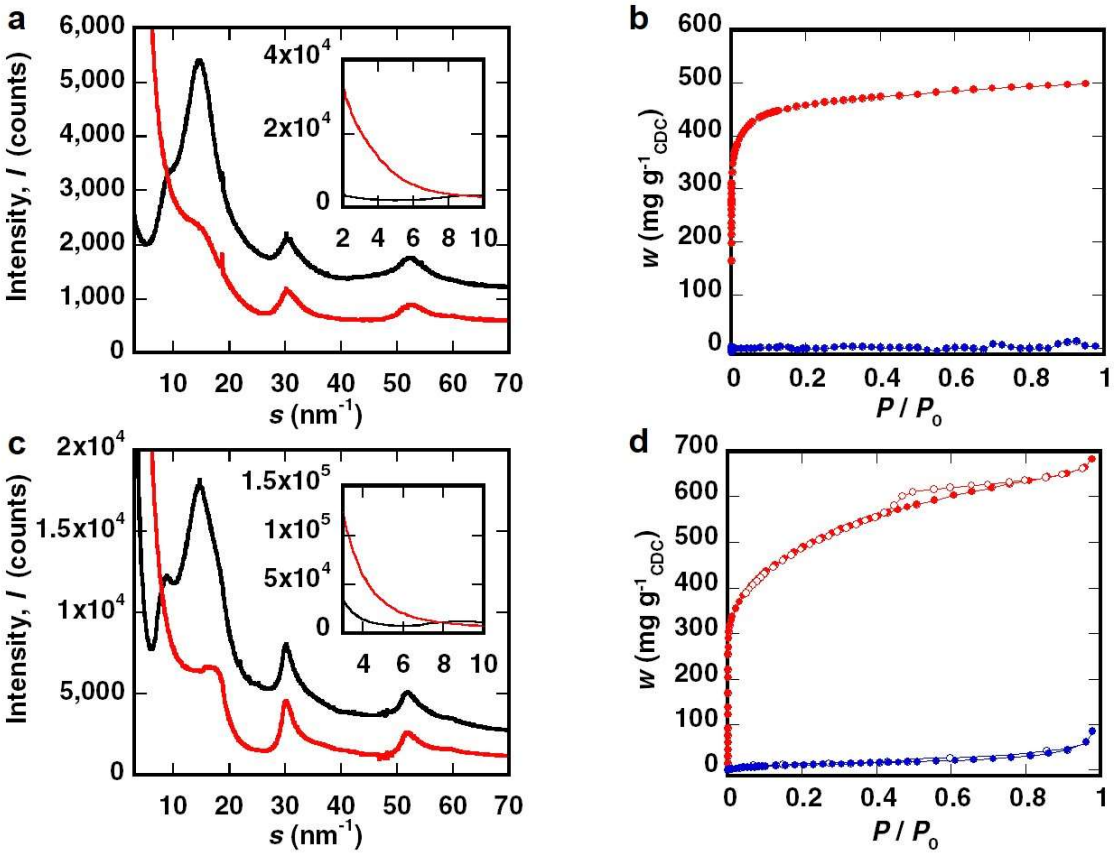

Figure S6| (**a**, **c**) X-ray scattering profiles of EMI-TFSI adsorbed CDCs (black) and of vacuum-treated CDCs (red) with 0.7-nm (**a**) and 1-nm (**c**) pore size. The small angle X-ray scattering regions are shown in the insets. (**b**, **d**) Nitrogen adsorption isotherms of EMI-TFSI containing adsorbed CDCs (blue) and EMI-TFSI-free CDCs powders (red) with 0.7-nm (**c**) and 1-nm (**d**) average pore size.

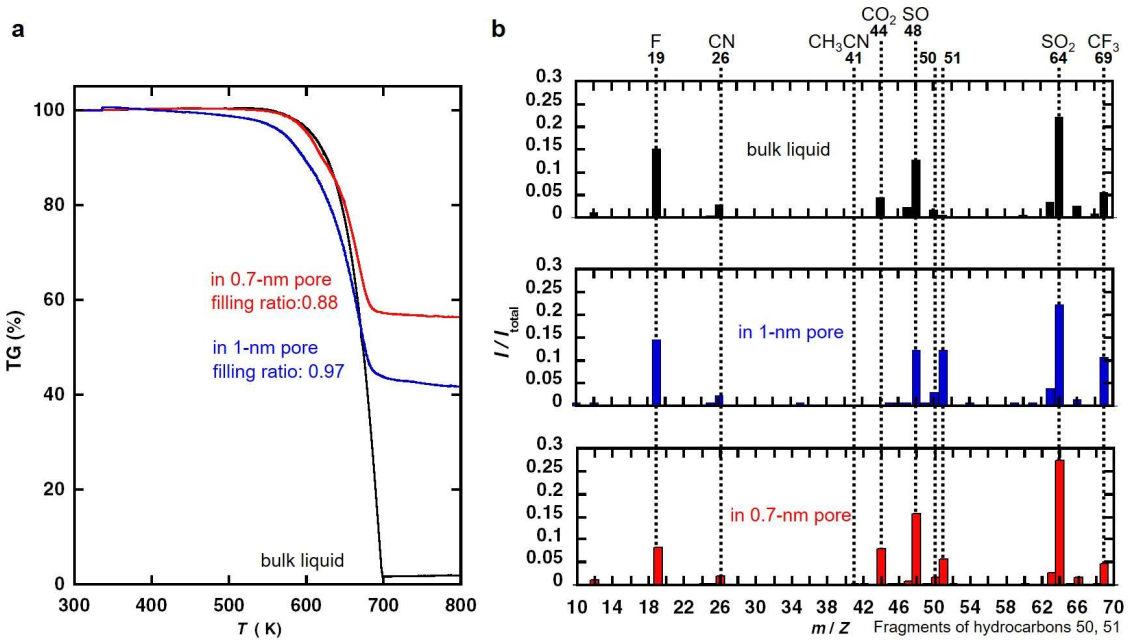

Figure S7| a, TG measurements of EMI-TFSI in bulk (black), 0.7-nm (red) and 1-nm (blue) pores of CDCs. **b**, Mass spectra of EMI-TFSI in bulk (black), 0.7-nm (red) and 1-nm (blue) pores of CDCs at decomposition temperatures of ca. 700 K.

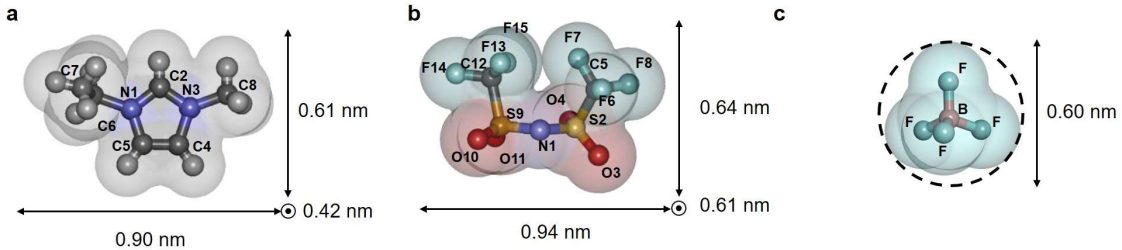

d

atom	σ (nm)	ε (kJ mol^{-1})	q (e)
N1	0.325	0.711	0.058
C2	0.355	0.293	-0.108
N3	0.325	0.711	0.159
C4	0.355	0.293	-0.120
C5	0.355	0.293	-0.125
C6	0.350	0.276	0.080
C7	0.350	0.276	-0.104
C8	0.350	0.276	-0.198
$H_{C2,4,5}$	0.242	0.126	0.210
HC6	0.250	0.126	0.067
HC7	0.250	0.126	0.137
HC8	0.250	0.126	0.061

e

atom	σ (nm)	ε (kJ mol^{-1})	q (e)
N1	0.325	0.711	-0.674
S2	0.355	1.046	1.049
O3	0.296	0.879	-0.542
O4	0.296	0.879	-0.521
C5	0.350	0.276	0.269
F6,7,8,13,14,15	0.295	0.222	-0.138
S9	0.355	1.046	0.995
O10	0.296	0.879	-0.512
O11	0.296	0.879	-0.534
C12	0.350	0.276	0.298

f

atom	σ (nm)	ε (kJ mol^{-1})	q (e)
B	0.358	0.397	1.1504
F	0.312	0.255	-0.5376

Figure S8| (**a**, **b, c**) Molecular structure and parameters[1,13] (**d**, **e, f**) used in HRMC simulation of (**a**) EMI, (**b**) TFSI and (c) BF_4 ions.

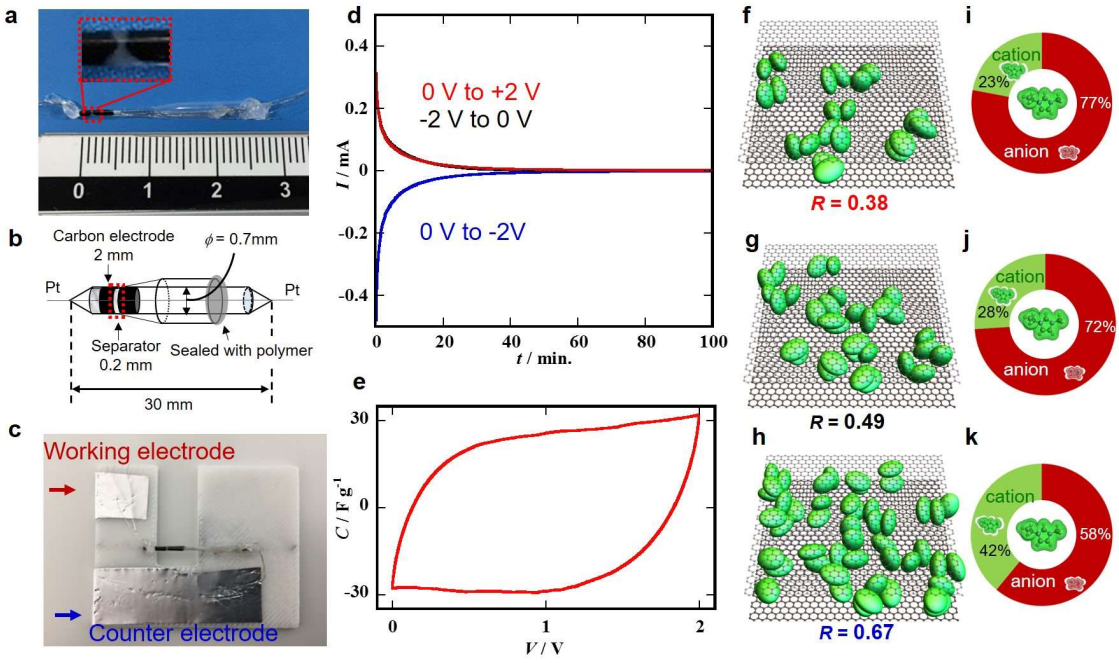

Figure S9| In-situ X-ray scattering cell for electrochemical measurement under polarization and effect of polarization on cation-cation structural anomaly (**a**) Picture of the in-situ X-ray scattering cell used to run the experiments. Inset: magnified photo of the center of the cell. (**b**) Schematic of the cell. (**c**) The electrochemical cell in a plastic cell folder with the positive and negative tabs to be placed into the goniometer in the synchrotron X-ray beam line BL5S2 (Aichi Synchrotron radiation facility). (**d**) Chronoamperometry during constant polarization at -2 V (blue), 0 V and +2 V (red). In-situ X-ray scattering measurements were performed after 1.5 h polarization, once steady-state condition (constant leakage current) was reached. (**e**) Cyclic Voltammogram of the in-situ X-ray scattering cell at a potential scan rate of 0.5 mV/s, showing a typical capacitive electrochemical signature; the carbon capacitance was

calculated as 100 $F.g^{-1}$, thus validating the cell design. (**f, g, h**) Snapshots of co-ion pairs of cations of EMI-TFSI in the 0.7 nm-pore at +2 V (**f**), 0 V (**g**) and -2 V (**h**) constant cell voltage. *R* is the ratio of paired cation number to total cation number. EMI cations are shown as green ellipsoids. (**i, j, k**) Population in the first coordination shell around an EMI cation in the 0.7 nm-pore under +2 V (**i**), 0 V (**j**) and -2 V (**k**).

8. Supplementary References

1. Fujii, K. *et al.* Liquid structure of room-temperature ionic liquid, 1-ethyl-3-methylimidasolium bis-(trifluoromethanesulfonyl) imide. *J. Phys. Chem. B* **112**, 4329-4336 (2008).

2. Lopes, J. N. C. & Padua, A. A. H. Nanostructural organization of ionic liquids. *J. Phys. Chem. B*, **110**, 3330-3335 (2006).

3. Klug, H. P. & Alexander, L. E. *X-Ray Diffraction Procedures: For Polycrystalline and Amorphous Materials* (Wiley-Interscience, New York, 1974).

4. Neimark, A. V. Lin, Y. Ravikovitch, P. I. & Thommes, M. Quenched solid density functional theory and pore size analysis of micro-mesoporous carbons. *Carbon* **47**, 1617-1628 (2009).

5. Kaneko,K. Ishii, C. Ruike, M. & Kuwabara, H. Origin of superhigh surface area and microcrystalline graphitic structures of activated carbons. *Carbon 30*, 1075-1088 (1992).

6. Wang, Z. M. & Kaneko, K. Dipole oriented states of SO_2 confined in a slit-shaped graphitic subnanospace from calorimetry. *J. Phys. Chem.* **99**, 16714-16721 (1995).

7. Setoyama, N. Kaneko, K. & Rodriguez-Reinoso, F. Ultramicropore characterization of microporous carbons at low-temperature helium adsorption. *J. Phys. Chem*. **100**, 10331-10336 (1996).

8. Suzuki, T. Kaneko, K. & Gubbins, K. E. Pore width-sensitive filling mechanism for CCl_4 in a graphitic micropore by computer simulation. *Langmuir* **13**, 2545-2549 (1997)

9. Kanoh, H. & Kaneko, K. Random magnetism of O_2 confined in a slit-shaped graphitic nanospace at low temperature. *J. Phys. Chem.* **99**, 5746-5749 (1995).

10. Setoyama, N. Suzuki, T. & Kaneko, K. Simulation study on relationship between high resolution αs-plot and pore size distribution for activated carbon. *Carbon* **36**, 1459-1467 (1998).

11. Radhkrishnan, R. Gubbins, K. Watanabe, E. A. & Kaneko, K. Freezing of simple fluids in microporous activated carbon fibers: Comparison of simulation and experiment. *J. Chem. Phys.* **111**, 9058-9067 (1999).

12. Choudhury, A. R. Winterton, N. Steiner, A. Cooper, A. I. & Johnson, K. A. *In situ* crystallization of ionic liquids with melting points below -25°C. *Cryst. Eng. Comm.* **8**, 742–745 (2006).

13. Lopes, J. N. C. Deschamps & J. Pádua, A. A. H. Modeling ionic liquids using a systematic all-atom force field. *J. Phys. Chem. B*, **108**, 2038-2047 (2004)